# Monomolecular and Bimolecular Recombination of Electron–Hole Pairs at the Interface of a Bilayer Organic Solar Cell

*Tobias Hahn, Steffen Tscheuschner, Frank-Julian Kahle, Markus Reichenberger, Stavros Athanasopoulos, Christina Saller, Guillermo C. Bazan, Thuc-Quyen Nguyen, Peter Strohriegl, Heinz Bässler, and Anna Köhler*

**While it has been argued that field-dependent geminate pair recombina-tion (GR) is important, this process is often disregarded when analyzing the recombination kinetics in bulk heterojunction organic solar cells (OSCs). To differentiate between the contributions of GR and nongeminate recom-bination (NGR) the authors study bilayer OSCs using either a PCDTBT-type polymer layer with a thickness from 14 to 66 nm or a 60 nm thick p-DTS(FBTTh$_2$)$_2$ layer as donor material and C$_{60}$ as acceptor. The authors measure *JV*-characteristics as a function of intensity and charge-extraction-by-linearly-increasing-voltage-type hole mobilities. The experiments have been complemented by Monte Carlo simulations. The authors find that fill factor (FF) decreases with increasing donor layer thickness ($L_p$) even at the lowest light intensities where geminate recombination dominates. The authors inter-pret this in terms of thickness dependent back diffusion of holes toward their siblings at the donor–acceptor interface that are already beyond the Langevin capture sphere rather than to charge accumulation at the donor–acceptor interface. This effect is absent in the p-DTS(FBTTh$_2$)$_2$ diode in which the hole mobility is by two orders of magnitude higher. At higher light intensities, NGR occurs as evidenced by the evolution of s-shape of the *JV*-curves and the concomitant additional decrease of the FF with increasing layer thickness.**

## 1. Introduction

The power conversion efficiency in organic solar cells (OSCs) depends in a complex way on several parameters, i.e., (i) the fraction of the solar spectrum that is absorbed in the cell, (ii) the prob-ability that an absorbed photon creates a Coulomb-bound pair of charge carriers,(iii) the internal electric field needed to dissociate that electron–hole pair (eh-pair), (iv) the fraction of charge car-riers that escapes bimolecular recombina-tion before reaching the electrodes, and (v) the contact resistance that can impede charge extraction at the electrodes.[1–3] A measure of the fraction of the photo-generated charges that are actually collected at the electrodes is the fill factor (FF).[4–11] Its value thus directly reflects the mechanism of charge carrier genera-tion, which is a controversially discussed issue in the organic photovoltaic (OPV) community. By definition, the FF gives an indication on the voltage dependence of the photo current in the range between zero applied voltage and the open-circuit voltage.

Traditional models for the photogeneration of charges,[12] and thus also for the photocurrent–voltage (*JV*) curves, have always taken into account that an electric field is needed to dissociate the interfacial eh-pair, be it in bulk heterojunc-tion (BHJ)[8,13] or in planar heterojunction (PHJ)[14,15] solar cells. This implies that the inverse process, geminate recom-bination (GR), plays a role in controlling the shape of the *JV*-curves. The significant influence of electric field assisted dissociation and, conversely, geminate recombination has been well established experimentally for both PHJ cells[16,17] and BHJ cells.[18–20] In recent years, however, there has been an increasing number of reports demonstrating that device performance, and concomitantly the FF, is dominated by non-geminate recombination (NGR) processes such as Langevin or Shockley–Read–Hall-type recombination.[21–26] Moreover, the appearance of an s-shaped kink in the *JV*-curves of PHJ cells has been associated with the prevalence of NGR, provided that injection or extraction barrier effects can be excluded.[27,28] The NGR is considered to arise from charge accumulation at the heterojunction interface.[24] What causes a significant

contribution of either geminate or nongeminate recombination, and which factors determine the relative weight of both recombination pathways has been addressed by a few groups.[19,29–34] These groups find distinct branching ratios between GR and NGR that change with film morphology, so that it can be influenced by appropriate processing conditions. Nevertheless, a microscopic understanding of what controls these recombination pathways is still lacking.

Here we have analyzed $JV$-curves of PHJ cells made with different donor layer thicknesses ($L_p$) from 14 to 66 nm covered by a 30 nm thick $C_{60}$ layer as acceptor, sandwiched between ITO/$MoO_3$ and Al electrodes. The donor material $PCZ_{0.3}$ is a statistical low bandgap copolymer of the PCDTBT family shown in **Figure 1**. For brevity, we shall refer to it as $PCDTBT_{stat}$. The results are compared to PHJ cells employing the molecular donor p-DTS(FBTTh$_2$)$_2$. We show that the branching ratio between GR and NGR depends not only on operational parameters such as light intensity and electric field but also on device parameters such as film thickness. Using Monte Carlo (MC) simulations we illustrate how, close to the open-circuit condition, not only nongeminate recombination, but also the rate of geminate recombination depends on the competition between diffusive motion toward the collecting electrode and toward the sibling countercharge. The role of mobility and delocalization of charges is discussed. These results advance our microscopic understanding of the charge generation process which is the basis for the fabrication of efficient solar cells.
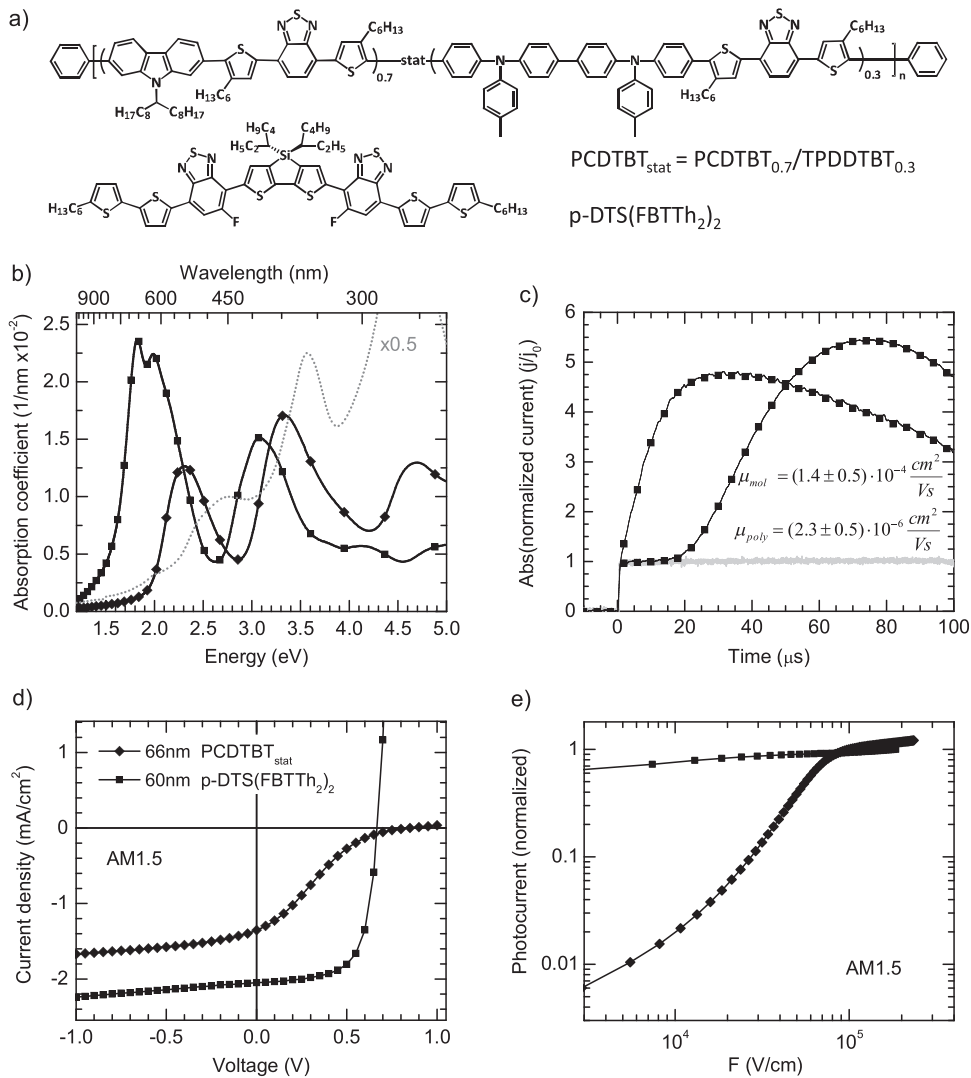


**Figure 1.** a) Chemical structure of the polymeric PCDTBT$_{stat}$ and the oligomeric p-DTS(FBTTh$_2$)$_2$ donor materials and b) the absorption coefficients of PCDTBT$_{stat}$ (gray diamonds), p-DTS(FBTTh$_2$)$_2$ (black squares) and C$_{60}$, measured from a 30 nm thick film. c) The current–response curves obtained in an MIS-CELIV measurement for PCDTBT$_{stat}$ and for p-DTS(FBTTh$_2$)$_2$, as well as the response of the samples when no offset is applied (gray line). The extracted mobilities are given in the figure. d) The current as a function of applied voltage under AM1.5 sun light conditions for a bilayer cell with 66 nm of PCDTBT$_{stat}$ donor and for an identical bilayer cell made with 60 nm of p-DTS(FBTTh$_2$)$_2$ as donor. e) The photocurrent obtained from (d) replotted as a function of internal field.

## 2. Results

Tress et al. suggested that mobility imbalance between electron and holes would be a major factor contributing to an s-shape in the $JV$-characteristics of PHJ cells.[27] In order to probe this hypothesis and to illustrate its effect we measured the $JV$-characteristics of two bilayer diodes, each made with a 60–66 nm thick low bandgap donor layer covered by a 30 nm thick $C_{60}$ acceptor layer sandwiched between an $ITO/MoO_3$ anode and an Al cathode. The chemical structures and absorption spectra of the donor materials, i.e., the molecule p-DTS(FBTTh$_2$)$_2$ and the polymer PCDTBT$_{stat}$, are shown in Figure 1a,b. Both materials form suitable heterojunctions with $C_{60}$, since $C_{60}$ has HOMO and LUMO levels of −6.4 and −3.7 eV, while the corresponding values for the donors are −5.12 and −3.34 eV for the p-DTS(FBTTh$_2$)$_2$ and −5.2 and −2.9 eV for PCDTBT$_{stat}$.[35–40] A key difference between the two materials is their hole mobility. We used the metal–insulator–semiconductor charge-extraction-by-linearly-increasing-voltage (MIS-CELIV) approach to determine specifically the hole mobility in each donor (Figure 1c). For p-DTS(FBTTh$_2$)$_2$, we obtain a value of $1.4 \pm 0.5 \times 10^{-4}$ cm$^2$ V$^{-1}$ s$^{-1}$, while only $2.3 \pm 0.5 \times 10^{-6}$ cm$^2$ V$^{-1}$ s$^{-1}$ are obtained for the hole mobility in PCDTBT$_{stat}$. The latter value is about three orders of magnitude lower than the electron mobility in $C_{60}$, which is in the range of $10^{-3}$–$10^{-2}$ cm$^2$ V$^{-1}$ s$^{-1}$.[41] Indeed, under AM1.5 illumination (Figure 1d), the $JV$-characteristics of the bilayer diode with the PCDTBT$_{stat}$ is s-shaped with a fill-factor of merely 22%, in contrast to the diode with p-DTS(FBTTh$_2$)$_2$, that has a fill-factor of 67%. This difference is also evident when replotting the $JV$-curves as field dependence of the photocurrent (Figure 1e), as described further below. While these data clearly confirm the notion that the magnitude of hole mobility has an important bearing of the diode performance, it is not fully understood how this relates to the underlying microscopic mechanism.

To address the microscopic reason, we consider the $JV$-curves of the bilayer as a function of the layer thickness of the donor for the PCDTBT$_{stat}$ (**Figure 2**), in the dark as well as both for broadband excitation at AM1.5 (100 mW cm$^{-2}$) and for monochromatic excitation. The thickness of the $C_{60}$ acceptor layer was kept at 30 nm while the donor layer thickness was varied from 14 to 66 nm. The dark current characteristics for the diodes (Figure 2a) are a superposition of an ohmic leakage current that is symmetric about $V = 0$ V and an injection current that increases steeply with voltage above $\approx 0.6$ V and with decreasing thickness of the donor layer. This strong voltage dependence of the forward current on the donor thickness is an indication that it is controlled by the space charge injected from the ohmic $ITO/MoO_3$ anode. Thus, the dark $JV$-curves are perfectly "well-behaved" and they are tractable in terms of drift-diffusion theory developed by Wetzelaer et al.[42,43]

Under illumination, the highest short circuit current $j_{SC}$, 2.2 mA cm$^{-2}$, is obtained for the thinnest diode using broad band excitation at air mass 1.5 (AM1.5), shown in Figure 2b. Considering that in a bilayer OSC only excitations generated within a 5–10 nm exciton diffusion range to the bilayer contribute to the photocurrent, this is a remarkably high value. The short circuit current decreases slightly when the thickness $L_p$ of the polymer layer increases, approaching a value of
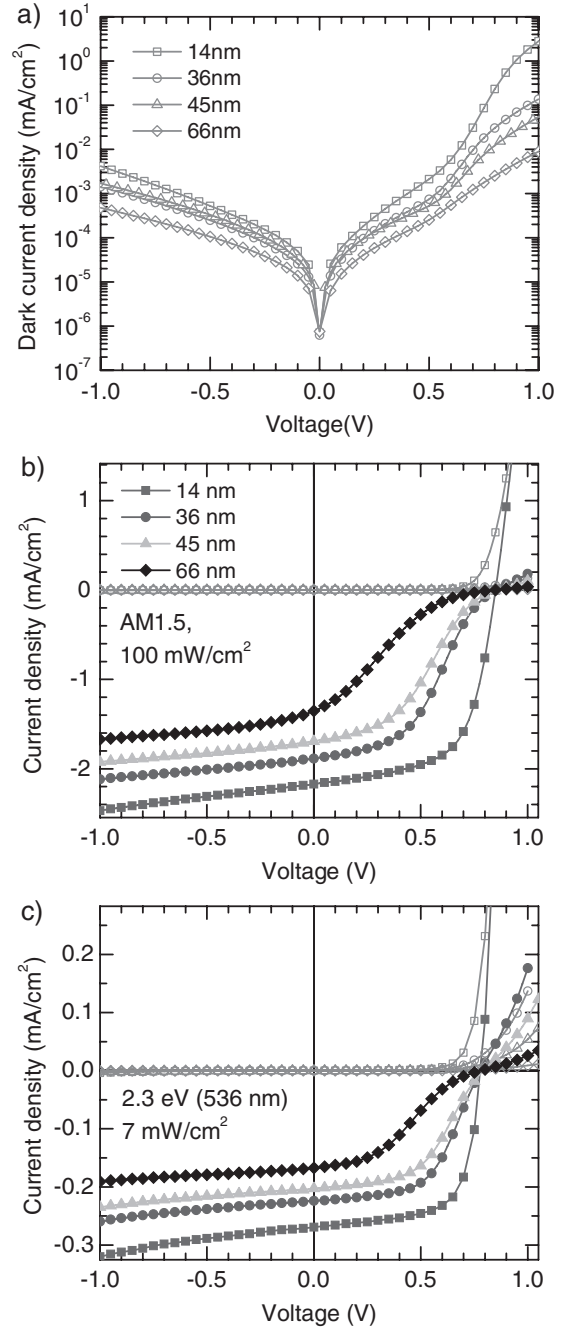
**Figure 2.** Current–voltage characteristics for different polymer layer thicknesses, i.e., 14 nm (squares), 36 nm (circles), 45 nm (triangles), 66 nm (diamonds), measured a) in the dark, b) under broadband excitation at AM1.5, and c) under monochromatic excitation at 536 nm (2.3 eV) at 7 mW cm$^{-2}$. The filled symbols show the total current under illumination and the open symbols the dark current for each polymer layer thickness.

1.5 mA cm$^{-2}$ for the diode with $L_p = 66$ nm. More importantly, with increasing thickness of the donor layer the $JV$-curves acquire an s-shape character. Since the only variable parameter of the diodes is the thickness of the donor layer it appears straightforward to associate the evolution of the s-shape character of the $JV$-curves upon increasing $L_p$ with charge carrier

3

recombination rather than with injection or extraction barriers.[28] These experimental results at AM1.5 are consistent with reports by Yu et al. for PHJ cells made with SubPc and $C_{60}$, for donor thicknesses from 10 to 40 nm,[24] and with reports by Petersen et al., for PHJ cells using a merocyanine dye as donor and $C_{60}$ as acceptor.[17] It seems that this recombination effect depends on hole mobility since the s-shape of the JV-curve is lost when the PCDTBT$_{stat}$ is replaced by the p-DTS(FBTTh$_2$)$_2$ that has an almost 100 times higher hole mobility (Figure 1d). A similar thickness-dependence of the s-shape also appears upon monochromatic excitation of 7 mW cm$^{-2}$ of predominantly the donor at the maximum of its first absorption band (536 nm, about 2.3 eV), though it sets in at higher voltages.

Similar results are obtained for excitation at 580 nm (2.1 eV, see Figure S2 in the Supporting Information). Since the $C_{60}$ still absorbs weakly at 2.3 eV, yet it does not absorb at 2.1 eV (see Figure 1), all subsequent monochromatic measurements were carried out at 2.1 eV. The radiant flux of 2.1 eV photons impinging on the sample is 6.7 mW cm$^{-2}$.

A straightforward way to check whether or not the evolution of the s-shape PCDTBT$_{stat}$/$C_{60}$ diodes is indeed caused by charge carrier recombination is to measure the dependence of the photocurrent as a function of light intensity. **Figure 3**a shows that the short circuit photocurrents, measured at a photon energy of 2.1 eV (580 nm), are perfectly linear with incident light intensity up to 30 mW cm$^{-2}$ and even up to 100 mW cm$^{-2}$ broadband
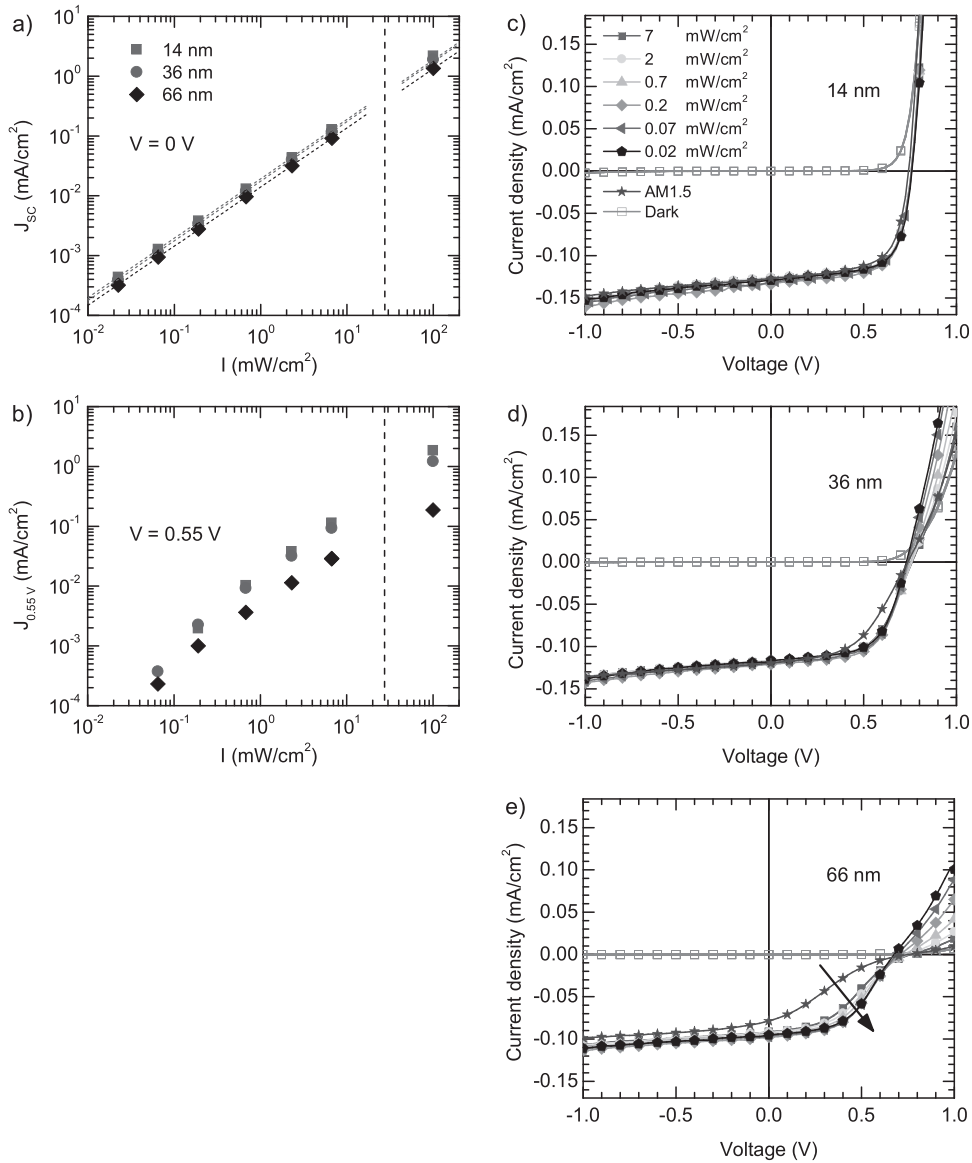


**Figure 3.** The total current as a function of illumination intensity, measured a) under short-circuit conditions ($V = 0$ V) and b) at $V = 0.55$ V. Values up to 30 mW cm$^{-2}$ are for monochromatic illumination at 580 nm (2.1 eV), and values at 100 mW cm$^{-2}$ are for broadband excitation at AM1.5. The dotted lines indicate a linear fit of the data points below 30 mW cm$^{-2}$. For a c) 14 nm, d) 36 nm, and e) 66 nm thick polymer layer current–voltage characteristics are shown for different light intensities at 580 nm and AM1.5 illumination. The JV-characteristics are normalized as described in the text.

excitation (AM1.5), suggesting that virtually no carriers are lost by bimolecular recombination. In contrast, when measuring the photocurrent closer to the open-circuit voltage, e.g., at 0.55 V (Figure 3b), we observe a deviation from linearity that implies that bimolecular processes are now dominant.

We can use the observed linear dependence of $j_{SC}$ to normalize our $JV$-curves to $j_{SC}$, such as to compare their shapes. In Figure 3c–e, we thus assess how the light intensity affects the photocurrents as a function of voltage for different film thicknesses. Usually, comparing the $JV$-curves of solar cells under different high intensity illuminations is straightforward since in each case the dark current characteristic is negligible. A negligible contribution of the dark current is also tacitly assumed when calculating the fill factor, usually defined as the product of current and voltage at the maximum power point divided by the product of short-circuit current and open-circuit voltage.[1] However, this assumption is no longer valid when the light intensity decreases by up to three orders of magnitude because the dark current stays constant while the photocurrent decreases until the photocurrent eventually becomes comparable or even smaller than the dark current. In order to avoid any artifacts associated with the dark current we subtracted the dark current from the total current, thus obtaining the photocurrent. This photocurrent was then normalized to the light intensity $I_0 = 6.7$ mW cm$^{-2}$ and the dark current was added again. Thus, the normalized current is given by

$$j_{normalized}(V) = \left[ j_{photo}(V) \cdot \frac{I_0}{I} \right] + j_{dark} \qquad (1)$$

where $j_{photo}$ is the photocurrent obtained under illumination with intensity $I$, $j_{dark}$ is the dark current, and $I_0$ is our reference intensity $I_0 = 6.7$ mW cm$^{-2}$. Note that if instead we had normalized the $JV$-curves of the total current, we would also have implicitly multiplied the dark current by the normalization factor $\frac{I_0}{I}$, thus introducing an artefact, and this is avoided by subtracting the dark current prior to the normalization and then adding it again afterwards.

Figure 3c–e compares the $JV$-curves obtained for different light intensities, normalized as just described to illumination with $I_0 = 6.7$ mW cm$^{-2}$, for different film thicknesses. We focus on the voltage range between $V = 0$ V and $V = V_{OC}$. It is evident that, as $V$ approaches $V_{OC}$, the $JV$-characteristics become more intensity dependent as the donor thickness increases. For diodes with 14 nm, the $JV$-curve normalized to light intensity are indistinguishable, indicating that bimolecular effects cannot be important. For $L_p = 36$ nm diodes, some deviation is seen upon increasing the intensity (Figure 3d) and, for $L_p = 66$ nm, an s-shape develops (Figure 3e). The effect is more pronounced when the data measured under AM1.5 illumination are included. Figure 3 confirms that in the thicker diode bimolecular recombination becomes a loss process for photocarriers while this is not the case in the thinnest diode.

From Figure 3, we can read out the fill factor as a function of light intensity, shown in **Figure 4**. We find that for the $L_p = 14$ nm diode, the FF remains constant at about 67% as the illumination intensity changes by four orders of magnitude. For the $L_p = 36$ nm diode, the FF decreases from 61% to 50%
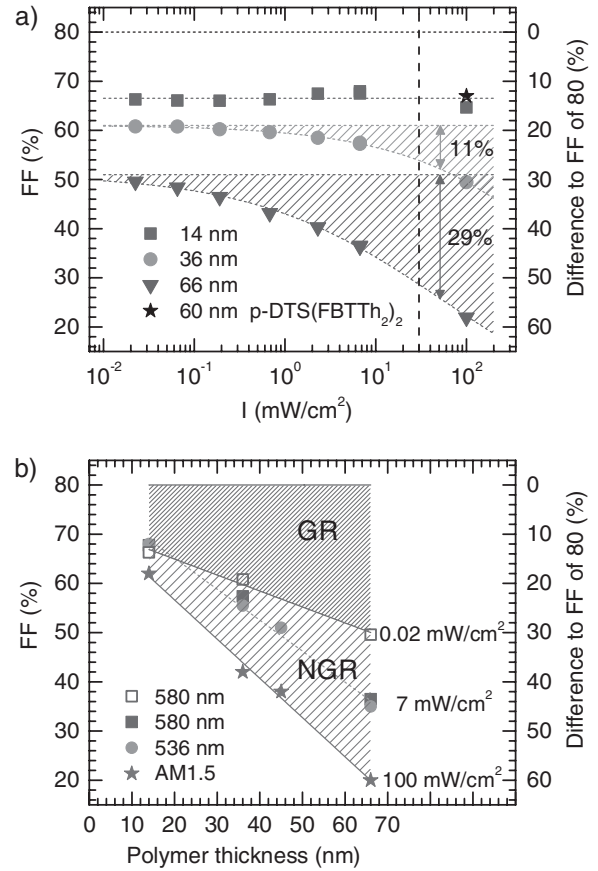


**Figure 4.** a) Fill factor for a polymer thickness of 14, 36, and 66 nm for different light intensities at an excitation wavelength of 580 nm. Dotted lines serve as guide to the eye. The fill factor obtained with AM1.5 illumination is also shown (on the right side of the dashed vertical line). The FF was calculated using the $JV$-curves shown in Figure 3. The fill factor for an identical bilayer cell made with 60 nm of the oligomer p-DTS(FBTTh$_2$)$_2$ is also shown (black star). On the right axis, the difference to an assumed ideal fill factor of 80% is indicated. The colored horizontal lines indicate the asymptotic value of the data at each thickness for infinitely low illumination, obtained by extrapolation of a fit to the data. The difference between the horizontal lines and 80% is attributed to losses due to geminate recombination, and the difference between the horizontal lines and the data points (shaded area) is attributed to losses by nongeminate recombination. The vertical arrows and associated numbers indicate the NGR losses at AM1.5 (the arrows are slightly offset from 100 mW cm$^{-2}$ for clarity of display). b) Fill factors for different light intensities as a function of polymer layer thickness. The difference in FF between the data obtained at 0.02 mW cm$^{-2}$ to 80% (densely shaded area) is attributed to losses by geminate recombination, and the difference between the data at 0.02 mW cm$^{-2}$ and the data obtained at higher intensities such as 100 mW cm$^{-2}$ is attributed to nongeminate recombination.

while in the 66 nm diode FF drops from 51% to 22% under AM1.5 (Figure 4a). For reference, we also include the FF of the 60 nm p-DTS(FBTTh$_2$)$_2$/C$_{60}$ diode, which is 67%, i.e., the same as in the 14 nm PCDTBT$_{stat}$/C$_{60}$ diode at any intensity.

Figure 4a allows to differentiate between the contributions of geminate and nongeminate recombination to the overall reduction in fill factor. Let us assume that, for an ideal cell in the Shockley–Queisser limit, the maximum obtainable fill factor is

80%, in agreement with simulations of Bartesaghi et al.[5] The difference to the FF actually observed in the limit of the lowest illumination intensity can be assigned to predominantly geminate recombination. In Figure 4a, this value is indicated by a dashed line for each film thickness. The difference to this value that arises with increasing illumination intensity, however, can be attributed to nongeminate recombination losses, indicated by the shaded areas in Figure 4a. Evidently, the FF is reduced by predominantly GR for the thinnest donor layer, while the losses due to GR and NGR are equal at AM1.5 for the thickest layer investigated.

How the fill factor decreases with the thickness of the donor layer is illustrated in Figure 4b. The contributions from GR and from NGR are indicated by the red and green areas. While the FF value for the thin sample is, within the experimental error, independent of intensity, with increasing film thickness a slopes arises not only for broadband illumination at AM1.5 but also for monochromatic illumination at 0.02 mW cm$^{-2}$, suggesting a thickness dependence of geminate recombination.

For the subsequent analysis it is useful to convert the $JV$-plots into plots of the photocurrent as a function of the internal electric field. We calculated the internal field $F$ according to $F = (V_{\text{build-in}} - V)/(L_p + L_{C60})$, where $L_p$ and $L_{C60}$, are the thicknesses of the polymer donor layer and the $C_{60}$ layer, $V$ is the voltage applied to the diode and $V_{\text{build-in}}$ is the voltage at which the photocurrent equals zero. In **Figure 5**a, we compare the field dependence of the photocurrents for different thicknesses of the donor layer taken under low light intensity and under AM1.5. The arrows indicate the field strengths corresponding to the short-circuit conditions for the OSCs with $L_p = 14$ nm and $L_p = 66$ nm, i.e., corresponding to $V = 0$ V. While the photocurrent is independent of electric field and illumination intensities for high internal fields, ($V < 0$ V), there is a strong field dependence of the photocurrent for low internal fields, even at very low illumination intensity, which reflects the field dependence of the dissociation of eh-pairs at the interface.[18] For reference, an internal field of $10^4$ V cm$^{-1}$ translates into a difference of less than 0.1 V to $V_{\text{build-in}}$.

This field dependence increases with light intensity and with increasing thickness of the polymer donor layer. The difference between the field dependent photocurrent for low and for high intensity, normalized to the current at AM1.5, is displayed in Figure 5b, from which the strong thickness dependence is particularly evident. Essentially, in Figure 5b, the current is corrected for the field dependence due to the geminate recombination, so that the data reflect the strong field and thickness dependence of the nongeminate recombination pathway. This difference between the photocurrent at high and low illumination intensities vanishes above saturation field $F_{\text{sat}}$ of the photocurrent. This is the field at which all primarily generated eh-pairs are dissociated and are extracted by the electrodes. For $F < F_{\text{sat}}$ an increasing fraction of eh-pairs execute a diffusive motion inside the coulombic capture sphere. They are thus able to return to their siblings. As their concentration increases due to more intense illumination, they find recombination partners that are not their siblings. Figure 5b shows that this nongeminate recombination is particularly field dependent for thick donor layers.

To further probe the effect of film thickness on the dissociation of CT states, we carried out Monte Carlo simulations. In
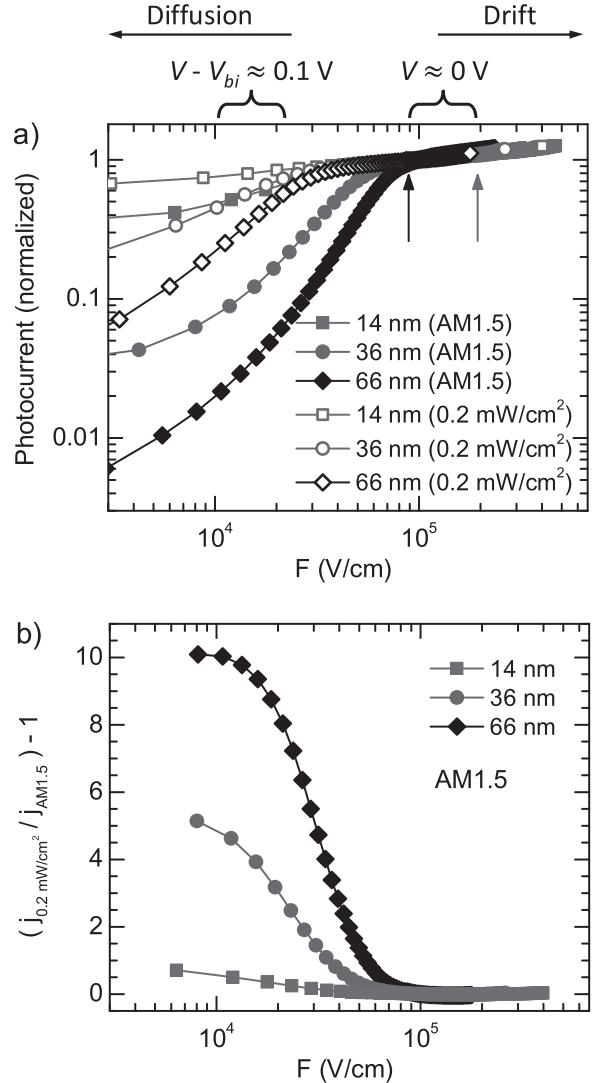


**Figure 5.** a) Photocurrent as a function of internal field $F = (V_{\text{build-in}} - V)/(L_p + L_{C60})$ for different polymer layer thicknesses, i.e., 14 nm (squares), 36 nm (circles), 45 nm (triangles), 66 nm (diamonds), taken under 580 nm illumination with an intensity of 0.2 mW cm$^{-2}$ (open symbols) and under AM1.5 illumination (filled symbols). The field is calculated using $V_{\text{build-in}} = 0.85$ V for all thicknesses at AM1.5 and $V_{\text{build-in}} = 0.76$, 0,74, and 0.71 V for $L_p = 14$, 36, and 66 nm for 580 nm excitation, respectively. The arrows indicate the field strengths corresponding to the internal field under short-circuit conditions for the OSCs with $L_p = 14$ nm (right arrow) and $L_p = 66$ nm (left arrow). b) Difference between photocurrent at 0.2 mW cm$^{-2}$ and at AM1.5, normalized to the photocurrent at AM1.5, $(j_{0.2} - j_{\text{AM1.5}})/j_{\text{AM1.5}}$, as a function of internal field for different film thicknesses.

order to simplify the simulation we considered a bilayer OSC composed of an array of point sites with variable thickness of the donor layer, assuming that the electron remains stationary in the acceptor layer. As detailed in the methodology, the quantum yield $\varphi(F)$ for electron–hole separation was calculated by averaging over $10^6$ individual trials. In each trial, we created a single electron–hole pair at the interface. We kept the electron stationary while allowing the hole to execute a random walk in the potential created by the mutual Coulomb attraction
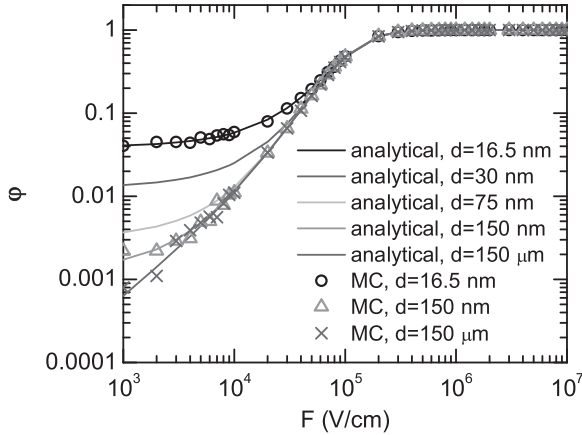
**Figure 6.** The probability of electron–hole separation as a function of internal field derived by Monte Carlo simulation (symbols) and derived by an analytical model (lines) for different thicknesses $L_p$ of the polymer layer as described in the text.

and the applied field. The trial was over when the hole reached either the collecting electrode or when it recombined with the electron. In this simulation, only monomolecular recombination is taken into account since only one electron–hole pair is considered for each trial. In addition to the MC simulations, we have also used an analytical expression to calculate the field dependent separation efficiency as developed by Rubel et al.[44] (see Section 5) which is in perfect agreement with the MC simulation. Compared to the experiment displayed in Figure 5, **Figure 6** shows that the simulations predict a qualitatively similar shape of the dissociation yield as a function of field and, moreover, a similar evolution with film thickness as observed experimentally. The simulations do, however, predict a larger saturation field than found in experiment because in the simulation we ignored the effect that a low effective mass of the conjugated polymer has on the dissociation yield.[45] However, this does not alter the conclusions regarding the thickness dependence of recombination at low fields. In Figure 6 we see that the photocurrent yield is enhanced when the thickness of the donor transport layer is of the order of the Langevin capture radius ($\approx 16$ nm) and the yield reduces considerably with thicknesses up to $\approx 150$ nm.

## 3. Discussion

Let us first summarize the essential experimental results. (i) In bilayer solar cells made with two different donors yet the same donor layer thickness of about 60 nm, a s-shape occurs for the donor with the lower hole mobility, yet not for the donor with the higher hole mobility, consistent with Tress et al.[27] (ii) The short circuit photocurrent in the bilayer diodes is linear with light intensity but when the applied voltage approaches $V_{OC}$, the $JV$-curves acquire s-shape character as the thickness of the donor layer increases (Figures 2 and 3). (iii) The fill factors increase and finally saturate at decreasing light intensity, and the saturation values decrease with increasing donor layer thickness (Figure 4). (iv) Losses in FF increase with increasing

film thickness for both, geminate recombination and nongeminate recombination. (v) Above a critical electric field, $F_{sat}$, the photocurrent is saturated. For $F < F_{sat}$, the photocurrent decreases. This effect is stronger (i.e., the slope $\mathrm{d}j/\mathrm{d}F$ is steeper) with increasing donor layer thickness and with increasing light intensity (Figure 5). (vi) The Monte Carlo simulations carried out in a strictly monomolecular regime reproduce the field and thickness dependence of the photocurrent that is experimentally observed.

Based upon the present experimental results we shall critically examine the role of monomolecular, i.e., geminate, recombination and of bimolecular, nongeminate recombination in organic solar cells, in particular with a view to the thickness dependence of the $JV$-curves.

The basic idea to account for the thickness dependence of the $JV$-curves is to consider the balance between charge extraction at the electrode and recombination of the electron–hole pair.[17,24] We stress that this is a field-dependent process. Let us first attend to the regime of very low excitation density, represented in the Monte Carlo simulation (Figure 6) and in the $JV$-curves under monochromatic illumination as displayed in Figures 2 and 5. After generation of an electron–hole pair, its hole diffuses in the combined potential of the Coulomb attraction by the electron and the internal field. If it does not leave the Langevin capture radius before recombining with the electron, i.e., if it has not truly been separated from its sibling electron, this is termed primary geminate recombination according to the IUPAC goldbook definition.[46] The Coulomb capture radius, i.e., the Langevin radius, is given by $r_{Coul} = \dfrac{e^2}{4\pi\epsilon\, k_B T}$, and it is about 16 nm for a material with dielectric constant of 3.5. We note that due to energetic disorder and charge delocalization this is not a well-defined, sharp boundary but rather a blurred out range. Primary geminate recombination does not play a role in the thickness dependence of the photocurrent yield, as in our case the polymer donor layer was always equal or larger than the Langevin capture radius. However, in particular at low internal fields, i.e., close to $V_{OC}$, it is also possible for the hole to separate from the electron by diffusing out of the Langevin capture radius, yet to enter it again at a later stage in its diffusive motion such as to return to its sibling electron. In chemical kinetics, recombination with the initial sibling countercharge after separation is known as secondary geminate recombination.[46]

Clearly, the rate of secondary geminate recombination depends on the thickness of the polymer donor layer. The thinner the polymer layer, the more likely it is that the hole in its diffusive motion meets the extracting electrode rather than returning to the electron. This is particularly true close to $V_{OC}$, i.e., in the low field regime, where the diffusive regime is prominent. The overall efficiency of geminate recombination is then controlled by the competition between a thickness-dependent charge extraction rate and a recombination rate that is independent of thickness. This is analogous to the well-known competition between NGR and extraction of free charges.[5] We therefore conclude that geminate recombination reduces the photocurrent close to $V_{OC}$, i.e., for low internal fields (Figure 5a), with this process being particularly important for thicker polymer donor layers. Geminate recombination thus is

also responsible for a reduction in fill factor (Figure 4a) under low light intensities, i.e., in the monomolecular regime.

We shall now discuss the evolution of the shape of the *JV*-curves as well the fill factor at higher light intensities. In addition to the monomolecular, geminate recombination processes, bimolecular processes can occur. The obvious process is nongeminate recombination from charges that, after photo-excitation, diffused out of their Langevin radius and return diffusively to the interface such as to recombine with another opposite charge there. The probability for this process increases with both light intensity and thickness of the donor layer. It will also become more probably for lower fields that enable diffusive return toward the interfacial layer. A further process that is possible is that one geminately bound pair can recombine with another geminately bound pair. While such a recombination of still primarily bound geminate pairs will also depend on intensity and field, it will not depend on film thickness. The ratio in the field dependence of the photocurrent for low and high intensity is displayed in Figure 5b. The stronger sensitivity to field for thick donor layers as compared to thinner donor layers thus directly reflects the increase in nongeminate recombination compared to the geminate recombination channel. For fields exceeding the saturation field, there is no thickness dependence since the charges are free, so that there is neither geminate nor nongeminate recombination.

So far, we have analyzed the *JV*-curve in the framework of considering geminate and nongeminate recombination. The appearance of an s-shape can, however, also be related to other factors. In particular, barriers to charge extraction or injection, as well as low or unbalanced carrier mobilities have been identified as causes for low fill factors and s-shaped *JV*-curves.[27,28,47,48] In our studies, the only parameter that has been varied was the thickness of the donor layer. The appearance of an s-shaped kink can therefore not be attributed to energy barriers or mobilities, as none of these change with film thickness.

Tress et al. further highlighted the role of low mobility and of imbalanced carrier mobility in reducing the fill factor of organic solar cells. Based on drift-diffusion simulations, Tress concludes that low carrier mobilities as well as imbalanced carrier mobilities lead to a high carrier density at the donor–acceptor interface, thus promoting recombination.[27] The key point of his argument is thus based on considering the carrier density. An increased recombination due to charge accumulation at the interface is also brought forward by Yu et al. to account for the appearance of an s-shape with donor layer thickness in SubPc/$C_{70}$ based PHJ cells.[24] Consistent with their reasoning, we also find that an increased excitation density enhances recombination by adding the NGR channel. However, our key argument goes beyond this and also applies in the limit of vanishing carrier density. Charge accumulation at the interface is not required to reduce the fill factor. This is important as it implies that the carrier density does not need to be high or even in the range of the capacitor charge for the FF to be reduced by recombination losses.[7]

Clearly, the rate of carrier extraction, which prevents recombination, increases with mobility, even in the limit of considering a single electron–hole pair prone to geminate recombination. In the diffusive regime near $V_{OC}$, the diffusion range $L_p$ depends on the diffusivity $D$ by $L_p = \sqrt{D\tau}$, with $\tau$ being the carrier lifetime. Diffusivity is directly proportional to the carrier mobility by the Einstein relation $eD = \mu kT$. The probability of a hole to diffuse to the collecting electrode rather than to return to its sibling electron, i.e., the extraction rate, therefore increases with mobility. In this way, increasing mobility increases the photocurrent yield near $V_{OC}$ and improves the fill factor even in the regime of low illumination intensity and in the limit of vanishing carrier density. This microscopic picture accounts for the observation by Proctor et al.,[31] that changes in morphology reduce both losses due to GR and NGR.

In a similar way, increasing the delocalization of charges should, and in fact does, also improve the extraction rate.[45,49–51] One factor that contributes to this is that excited states or charges that are well delocalized, i.e., with an extended wavefunction, can diffuse further in a disordered environment than localized charges due to geometric reasons.[52] A second, and perhaps more important factor relates to the fact that the binding energy of the eh-pair is reduced by an additional energy term when the eh-pair is more delocalized. In the case of on-chain wavefunction delocalization of a hole along a polymer chain, this additional energy arises from the zero-point oscillation of the delocalized hole in the pair potential. Mathematically, it can be expressed via a reduced effective mass of the hole, that can be as low as 0.1 times the electron mass for planarized or well-ordered polymers.[45,53] A similar effect can arise for crystalline assemblies of donor or acceptor molecules. An additional 200 meV of electrostatic energy has, for example, been reported by Gélinas et al. due to electron delocalization in ordered regions of the fullerene acceptor material.[50]

## 4. Conclusions

The stimulant for this work was that we wondered why in a thin bilayer OSC the fill factor can be as high as about 70% but decreases with increasing thickness of the polymeric donor layer ($L_p$). To this end we measured the *JV*-characteristics of bilayer diodes composed of $PCDTBT_{stat}$ donor layers with thicknesses ranging from 14 nm and 66 nm and a 30 nm thick $C_{60}$ acceptor layer and light intensities ranging from 0.02 to 100 mW cm$^{-2}$. We find that at low light intensities the diode characteristics is strictly linear in intensity but the fill factor decreases from 67% to 50% when the thickness of the donor layer $L_p$ increases from 14 nm to 66 nm. Supported by Monte Carlo simulations we argue that this decrease of FF is a signature of GR of holes that initially escaped from the Langevin capture sphere but can diffuse back toward the interface and can recombine with their siblings. The presence of an exit electrode prevents back diffusion. Therefore the trade-off between GR and charge extraction becomes thickness dependent up to a layer thickness of a multiple of the Langevin capture radius.

Since GR is ultimately limited by the nonradiative decay of the charge transfer states at the donor–acceptor interface, the efficiency of hole extraction should increase with hole diffusivity, i.e., hole mobility. Experiments with a diode in which the polymeric donor has been replaced by a 60 nm thick p-DTS(FBTTh$_2$)$_2$ layer that has an about 100 times higher hole mobility confirms this expectation. The FF of a 60 nm
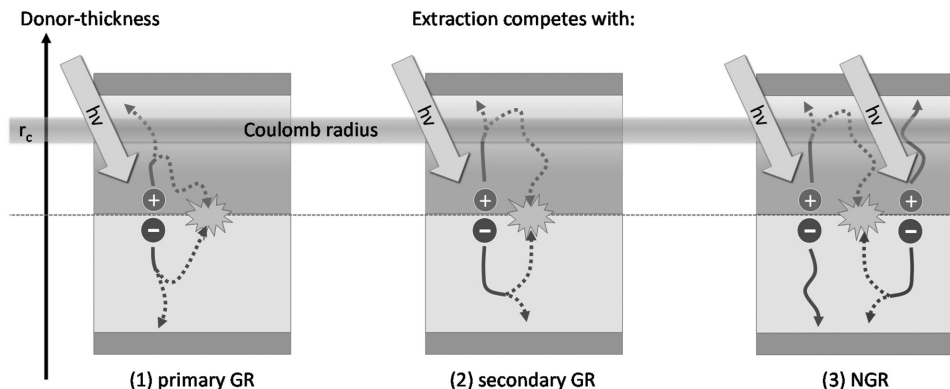
**Figure 7.** Schematic illustrating the competition between recombination at the donor–acceptor interface and extraction at the electrode for the mono-molecular process of geminate recombination and for the bimolecular process of nongeminate recombination. $r_c$ denotes the Coulomb capture radius (Langevin radius).

OSC with p-DTS(FBTTh$_2$)$_2$ at AM1.5 has a higher value than the FF of a PCDTBT$_{stat}$ OSC with same thickness at 0.02 mW cm$^{-2}$. Hence, the total losses of the p-DTS(FBTTh$_2$)$_2$ cell, i.e., GR and NGR, must be lower than the GR of the PCDTBT$_{stat}$ OSC (Figure 4). Thus, our results show that the limitation to the FF that is imposed by GR can be overcome by increasing the charge mobility. However, we stress that this effect is diffusion controlled, and consequently mobility controlled rather than controlled by interfacial charging, as is the case of NGR.[24]

As the light intensity increases and finally approaches AM1.5 the $JV$-curves acquire an s-shape that becomes more pronounced as the layer thickness increases. This is a signature of the onset of bimolecular, i.e., nongeminate recombination, at the donor–acceptor interface. As is well known, ultimately the diode efficiency is controlled by the trade-off between – the thickness dependent – extraction and NGR. The effect of NGR depends strongly on the internal electric field and film thickness (Figure 5b) due to interfacial charging.[24] Since the primary dissociation of charge transfer states at the interface is a field-assisted process, at lower electric field more eh-pairs exist near the donor–acceptor interface, so that a back-diffusing charge can easily find a recombination partner other than their siblings.

The overall picture is summarized in **Figure 7**. At low light intensity, a hole executing a random walk within the Coulomb capture radius of its electron may recombine with its sibling prior to any escape (primary GR). If it diffuses out of the Coulomb capture radius, it may be extracted at the electrode or it may diffuse back into the Coulomb capture radius such as to recombine with its sibling (secondary GR). Both processes are monomolecular. At high intensity, NGR will occur as additional, bimolecular process, as described above. In the framework of this microscopic picture it becomes evident why any process that improves charge carrier mobility, e.g., increasing the degree of (short-range) order in a film by processing, reduces not only losses due to NGR but also losses due to GR through enhancing the extraction rate.[31]

Our results show that simple $JV$-experiments of bilayer OSCs with variable layer thickness and variable light intensity provide a simple tool to quantify the effect of GR and NGR because the origins of recombination – be it geminate or nongeminate – and charge extraction are spatially separated.

## 5. Experimental Section

The compound p-DTS(FBTTh$_2$)$_2$ was synthesized as described by van der Poll et al.[35]

*Synthesis of the Polymer PCDTBT$_{0.7}$/TPDDTBT$_{0.3}$ (PCDTBT$_{stat}$):* PCDTBT$_{stat}$ (poly[(N-heptadecan-9'-yl)-2,7-carbazole-*alt*-5,5-(4',7'-bis-(4-hexylthien-2-yl)-2',1',3'-benzothiadiazole)]$_{0.7}$-*stat*-[N,N'-bis(4-methylphenyl)-N,N'-diphenylbenzidine-*alt*-5,5-(4',7''-bis-(4-hexylthien-2-yl)-2',1',3'-benzothiadiazole)]$_{0.3}$) was synthesized via Suzuki coupling according to the following procedure. The molar ratio of the carbazole, the phenyl-substituted benzidine, and the bisthienyl-benzothiadiazole units in PCDTBT$_{stat}$ was 0.7:0.3:1.

A Schlenk flask was charged with the monomers 2,7-bis-(4',4',5',5'-tetramethyl-1',3',2'-dioxaborolan-2'-yl)-N-(heptadecan-9''-yl)-carbazole (0.368 g, 0.560 mmol), N,N'-bis(4-methylphenyl)-N,N'-bis((4',4',5',5'-tetramethyl-1',3',2'-dioxaborolan-2'-yl)phenyl)-benzidine (0.184 g, 0.239 mmol), 4,7-bis(5'-bromo-4'-hexylthien-2'-yl)-2,1,3-benzothiadiazole (0.501 g, 0.800 mmol) and 12 mL of toluene under argon. One drop of Aliquat 336 and 20 mL of 2 M Na$_2$CO$_3$ solution were added and the mixture was degassed by three freeze–thaw cycles. Afterward 14 mg of tetrakis(triphenylphosphine)palladium(0) were added and followed by again three freeze–thaw cycles. The reaction mixture was then stirred under reflux in an argon atmosphere for 90 h before bromobenzene (0.126 g, 0.800 mmol) was added. After 2 h phenylboronic acid (0.098 g, 0.800 mmol) was added and the reaction mixture was again refluxed overnight. The reaction mixture was allowed to cool to room temperature and the polymer was precipitated into methanol/water (10:1). Soxhlet extraction was carried out using acetone and toluene. The reduced toluene fraction was precipitated into methanol/water (10:1) and dried in vacuum overnight, yielding 0.669 g (93%) of PCDTBT$_{stat}$ as a dark-red powder. A molecular weight of 47 000 gmol$^{-1}$ ($M_w$) and 18 000 gmol$^{-1}$ ($M_n$) was determined by size exclusion chromatography in THF solution with a polydispersity index of 2.56 (polystyrene calibration). The ionization potential was determined by photoelectron spectroscopy to be −5.2 eV. Adding the photon energy at maximum of the first absorption band yields −2.9 eV as a rough estimate for the ionization potential.

$^1$H NMR (300 MHz, C$_2$D$_2$Cl$_4$, 120 °C): $\delta$ = 0.75–0.95 (m, CH$_3$), 1.05–1.55 (m, CH$_2$), 1.75 (br, thiophene—CH$_2$), 2.04 (br, carbazole—CH$_2$), 2.23–2.44 (m, benzidine—CH$_3$, carbazole—CH$_2$), 2.63–2.95 (m, thiophene—CH$_2$), 4.62 (br, CH), 6.92–8.22 (m, ar—CH). Broadened and multiple signals were due to atropisomerism. From the integration of the signal for the CH$_2$ group in the swallow-tail spacer of the carbazole unit (2.04 ppm), the combined signal for the methyl group in the benzidine units and the other CH$_2$ group in the carbazole spacer (2.23–2.44 ppm), and the signal for the CH$_2$ groups in the hexyl spacer of the thiophene (1.75 ppm), a molar ratio of 0.7:0.3:1 was calculated (for $^1$H NMR spectrum see the Supporting Information).

*Experiments*: To fabricate the bilayer solar cells, ITO-coated substrates were covered with a patterned photoresist as described by Schwarz et al.[54] A 15 nm thick $MoO_3$ (Sigma Aldrich) layer was evaporated on top of it. The donor (PCDTBT$_{stat}$ or p-DTS(FBTTh$_2$)$_2$) was spun onto this from chlorobenzene solution (7.0 mg mL$^{-1}$). The thickness of the donor layer was controlled with a Dektak (Veeco) profilometer. T he donor was covered by subsequent thermal evaporation of a 30 nm thick $C_{60}$ layer and a 100 nm thick aluminium cathode. The devices were annealed at 140 °C for 15 min. The complete solar cell fabrication was done in a nitrogen atmosphere using a glovebox with direct access to the evaporation chamber. In Figure S1 in the Supporting Information, additional measurements were also carried out on samples where (i) the annealing step was omitted, or (ii) annealing was omitted and a 5 nm thick BCP layer was evaporated between $C_{60}$ and aluminum, or (iii) annealing was carried out for 15 min after $C_{60}$ evaporation, prior to deposition of a 5 nm thick BCP layer and aluminum. Since it turned out that the shape of the *JV*-curves is in dependent on the diode preparation the authors used annealed samples with the structure ITO/MoO$_3$/donor/C$_{60}$/Al since these feature particularly low dark current.

The current–voltage characteristics were measured in vacuum at room temperature under either broad band AM1.5 illumination employing a Newport sun simulator or under monochromatic illumination at 536 nm (2.3 eV) or 580 nm (2.1 eV), provided by a 450 W Xenon lamp (Osram) using a commercial monochromator. In the latter case the incident light intensity was varied by neutral optical density (OD) filters with optical densities of 0.5, 1.0, 1.5, 2.0, and 2.5. The light intensity impinging on the diode was measured using a Hamamatsu S1337-33BQ photodiode. Without OD filter, it was 7.1 mW cm$^{-2}$ for 536 nm and 6.7 mW cm$^{-2}$ for 580 nm. The photocurrents were measured with a Keithley 236 and 238 source-measure-unit.

To determine the fill factor of the photodiode at variable light intensities, both the dark current $j_{dark}(V)$ as well as the total current $j(V)$ under illumination were measured. The difference is the photocurrent $j_{photo}(V) = j(V) - j_{dark}(V)$. At low light intensities, one needs to take account of the fact that the dark current is independent on intensity while the photocurrent decreases with decreasing intensity. The authors did this by normalizing the photocurrent to the monochromatic light intensity without optical density (OD) filter. To do this, the photocurrent is multiplied by the ratio of the light intensity of monochromatic light without and with OD filters, and the dark current is added subsequently

$$j_{normalized}(V) = \left[ j_{photo}(V) \cdot \frac{I_0}{I} \right] + j_{dark} \qquad (2)$$

When the photocurrent is displayed as a function of internal field, the field was determined according to $F = (V_{build-in} - V)/(L_p - L_{C60})$, with $L_p$ being the layer of the polymer donor layer and $L_{C60}$ being the thickness of the $C_{60}$ acceptor layer (30 nm). The fields in the solar cells were calculated using $V_{build-in}$ which was approximated by the voltage at which the photocurrent equals zero.

MIS-CELIV measurements were performed according to the procedure described in literature.[55,56] For both materials the same parameters were used. The layer thickness of p-DTS(FBTTh$_2$)$_2$ was 100 nm and for PCDTBT$_{stat}$ 121 nm. A hole injection layer of 6 nm MoO$_3$ was used. The voltage was supplied by a Rigol DG4102 function generator. The slope of the voltage ramp, the offset voltage, and the length of the voltage pulse were fixed to 0.1 V µs$^{-1}$, 7 V, and 100 µs, respectively, for all measurements, to make sure that experimental conditions are identical for all compounds and samples. This ensures that observed trends and effects may be attributed to materials. The resulting current response signal was amplified using a Femto DHPCA-100 current amplifier and recorded with a Tektronix TDS3000 digital phosphor oscilloscope. In all the measurements the authors applied a prebias voltage of 7 V for one minute to ensure equilibrium conditions.

*Monte Carlo Simulations*: The authors performed Monte Carlo simulations to model the extraction efficiency in a bilayer device as a function of the electric field for different donor layer thicknesses. The system consisted of a 1D array of points with a separation distance $a = 1.5$ nm and an interface at origin. At $t = 0$ a hole and an electron

were placed in an adjacent configuration at the interface with a minimal separation. The electron position was fixed while the hole was allowed to move between neighboring points with a hopping rate $\nu_{i,j}$ given by a Miller–Abrahams expression

$$\nu_{i,j} = \begin{cases} \nu_0 e^{-2\alpha r_{ij}} e^{-\left( \frac{\varepsilon_j - \varepsilon_i}{k_B T} \right)}, & \varepsilon_j > \varepsilon_i \\ \nu_0 e^{-2\alpha r_{ij}}, & \varepsilon_j \leq \varepsilon_i \end{cases} \qquad (3)$$

where $i$ is the hole residence site and $j$ the target neighboring site, separated by a distance $r_{ij}$. The site energies $\varepsilon_i$ and $\varepsilon_j$ include contributions from the Coulomb potential due to the presence of the electron at the interface and the voltage drop due to the externally applied field. The attempt-to-hop frequency was set to $\nu_0 = 10$ ps$^{-1}$, the relative permittivity to $\epsilon_r = 4$, and the inverse localization length to $\alpha = 2$ nm$^{-1}$. At each Monte Carlo step the authors calculate a waiting time for each hopping event: $\tau_{ij} = -\frac{1}{\nu_{i,j}} \ln X$ and a waiting time for recombination between the electron–hole pair: $\tau_r = -\tau \ln X$, where $\tau$ is the electron–hole pair lifetime that increases exponentially with electron hole distance $r_{eh}$ as $\tau = \tau_0 e^{2\alpha(r_{eh} - a)}$ and $X$ is a random number from a box distribution between 0 and 1. The lifetime at close proximity is $\tau_0 = 1000 t_0$ with $t_0$ being the minimum hopping time $t_0 = \frac{1}{\nu_0} e^{2\alpha a}$.

The event with the smallest waiting time is is selected and executed. If the accepted event was a hop, then the authors updated the site of the hole and recalculated waiting times. If the chosen event was recombination, the authors removed the charges and started a new trial. Each trial terminated successfully when the electron–hole distance was larger than a given separation distance $d$, ranging from 16.5 nm to 150 µm. By averaging over $10^6$ trials the authors calculated the quantum yield for separation as: $\varphi(F) = \frac{N_{sep}(F)}{N_{tot}(F)}$, where $N_{sep}(F)$ is the number of successful trials for an applied field $F$ and $N_{tot}(F)$ the total number of trials.

The authors also used an analytical expression to calculate the field dependent separation efficiency $\varphi(F)$ as developed by Rubel et al.[44] This is derived from a rate equation model and reads

$$\varphi(F) = 1 - \frac{\sum_{i=1}^{n-1} \nu_{i,i+1}^{-1} e^{\left( \frac{\varepsilon_i - \varepsilon_1}{k_B T} \right)}}{\tau_0 + \sum_{i=1}^{n-1} \nu_{i,i+1}^{-1} e^{\left( \frac{\varepsilon_i - \varepsilon_1}{k_B T} \right)}} \qquad (4)$$

where $\varepsilon_1$ is the energy of the initially placed hole site at the interface right next to the electron and the index $i$ runs from 1 to $n - 1$ with $n$ being the site at distance $d$ from the interface at which the authors considered that the hole was separated. The forward, with respect to the field direction, hopping rates $\nu_{i,i+1}$ were given by the Miller–Abrahams expression described above.

## Supporting Information

Supporting Information is available from the Wiley Online Library or from the author.

## Acknowledgements

[1] A. Köhler, H. Bässler, *Electronic Processes in Organic Semiconductors: An Introduction*, Wiley-VCH, Weinheim, Germany, **2015**.

[2] P. Würfel, *Physics of Solar Cells*, Wiley-VCH, Weinheim, Germany, **2005**.

[3] N. C. Giebink, G. P. Wiederrecht, M. R. Wasielewski, S. R. Forrest, *Phys. Rev. B* **2011**, *83*, 195326.

[4] B. Liu, R. Q. Png, J. K. Tan, P. K. H. Ho, *Adv. Energy Mater.* **2014**, *4*, 1200972.

[5] D. Bartesaghi, I. D. Perez, J. Kniepert, S. Roland, M. Turbiez, D. Neher, L. J. A. Koster, *Nat. Commun.* **2015**, *6*, 7083.

[6] M. Stolterfoht, A. Armin, B. Philippa, R. D. White, P. L. Burn, P. Meredith, G. Juska, A. Pivrikas, *Sci. Rep.* **2015**, *5*, 9949.

[7] M. Stolterfoht, B. Philippa, S. Shoaee, H. Jin, W. Jiang, R. D. White, P. L. Burn, P. Meredith, A. Pivrikas, *J. Phys. Chem. C* **2015**, *119*, 26866.

[8] L. J. A. Koster, E. C. P. Smits, V. D. Mihailetchi, P. W. M. Blom, *Phys. Rev. B* **2005**, *72*, 085205.

[9] L. J. A. Koster, V. D. Mihailetchi, P. W. M. Blom, *Appl. Phys. Lett.* **2006**, *88*, 093511.

[10] P. W. M. Blom, V. D. Mihailetchi, L. J. A. Koster, D. E. Markov, *Adv. Mater.* **2007**, *19*, 1551.

[11] N. Christ, S. W. Kettlitz, S. Valouch, J. Mescher, M. Nintz, U. Lemmer, *Org. Electron* **2013**, *14*, 973.

[12] C. L. Braun, *J. Chem. Phys.* **1984**, *80*, 4157.

[13] V. D. Mihailetchi, L. J. A. Koster, J. C. Hummelen, P. W. M. Blom, *Phys. Rev. Lett.* **2004**, *93*, 216601.

[14] J. A. Barker, C. M. Ramsdale, N. C. Greenham, *Phys. Rev. B* **2003**, *67*, 075205.

[15] N. C. Giebink, B. E. Lassiter, G. P. Wiederrecht, M. R. Wasielewski, S. R. Forrest, *Phys. Rev. B* **2010**, *82*, 155306.

[16] A. Ojala, A. Petersen, A. Fuchs, R. Lovrincic, C. Polking, J. Trollmann, J. Hwang, C. Lennartz, H. Reichelt, H. W. Hoffken, A. Pucci, P. Erk, T. Kirchartz, F. Würthner, *Adv. Funct. Mater.* **2012**, *22*, 86.

[17] A. Petersen, A. Ojala, T. Kirchartz, T. A. Wagner, F. Würthner, U. Rau, *Phys. Rev. B* **2012**, *85*, 245208.

[18] R. A. Marsh, J. M. Hodgkiss, R. H. Friend, *Adv. Mater.* **2010**, *22*, 3672.

[19] S. Albrecht, W. Schindler, J. Kurpiers, J. Kniepert, J. C. Blakesley, I. Dumsch, S. Allard, K. Fostiropoulos, U. Scherf, D. Neher, *J. Phys. Chem. Lett.* **2012**, *3*, 640.

[20] D. Veldman, O. Ipek, S. C. J. Meskers, J. Sweelssen, M. M. Koetse, S. C. Veenstra, J. M. Kroon, S. S. van Bavel, J. Loos, R. A. J. Janssen, *J. Am. Chem. Soc.* **2008**, *130*, 7721.

[21] C. G. Shuttle, R. Hamilton, B. C. O'Regan, J. Nelson, J. R. Durrant, *Proc. Natl. Acad. Sci. USA* **2010**, *107*, 16448.

[22] T. M. Clarke, J. R. Durrant, *Chem. Rev.* **2010**, *110*, 6736.

[23] M. Gluecker, A. Foertig, V. Dyakonov, C. Deibel, *Phys. Status Solidi RRL* **2012**, *6*, 337.

[24] H. M. Yu, R. C. Yi, J. W. Zhang, A. R. Yu, H. Peng, J. J. Qin, X. Y. Hou, *J. Phys. D: Appl. Phys.* **2016**, *49*, 205105.

[25] D. Credgington, Y. Kim, J. Labram, T. D. Anthopoulos, J. R. Durrant, *J. Phys. Chem. Lett.* **2011**, *2*, 2759.

[26] R. Mauer, I. A. Howard, F. Laquai, *J. Phys. Chem. Lett.* **2010**, *1*, 3500.

[27] W. Tress, A. Petrich, M. Hummert, M. Hein, K. Leo, M. Riede, *Appl. Phys. Lett.* **2011**, *98*, 063301.

[28] W. Tress, A. Merten, M. Furno, M. Hein, K. Leo, M. Riede, *Adv. Energy Mater.* **2013**, *3*, 631.

[29] F. Etzold, I. A. Howard, R. Mauer, M. Meister, T. D. Kim, K. S. Lee, N. S. Baek, F. Laquai, *J. Am. Chem. Soc.* **2011**, *133*, 9469.

[30] A. Foertig, J. Kniepert, M. Gluecker, T. Brenner, V. Dyakonov, D. Neher, C. Deibel, *Adv. Funct. Mater.* **2014**, *24*, 1306.

[31] C. M. Proctor, S. Albrecht, M. Kuik, D. Neher, T. Q. Nguyen, *Adv. Energy Mater.* **2014**, *4*, 1400230.

[32] S. Albrecht, J. R. Tumbleston, S. Janietz, I. Dumsch, S. Allard, U. Scherf, H. Ade, D. Neher, *J. Phys. Chem. Lett.* **2014**, *5*, 1131.

[33] S. Albrecht, S. Janietz, W. Schindler, J. Frisch, J. Kurpiers, J. Kniepert, S. Inal, P. Pingel, K. Fostiropoulos, N. Koch, D. Neher, *J. Am. Chem. Soc.* **2012**, *134*, 14932.

[34] F. Gao, J. P. Wang, J. C. Blakesley, I. C. Hwang, Z. Li, N. C. Greenham, *Adv. Energy Mater.* **2012**, *2*, 956.

[35] T. S. van der Poll, J. A. Love, T. Q. Nguyen, G. C. Bazan, *Adv. Mater.* **2012**, *24*, 3646.

[36] M. A. Faist, T. Kirchartz, W. Gong, R. S. Ashraf, I. McCulloch, J. C. de Mello, N. J. Ekins-Daukes, D. D. C. Bradley, J. Nelson, *J. Am. Chem. Soc.* **2012**, *134*, 685.

[37] J. H. Seo, S. J. Kang, C. Y. Kim, S. W. Cho, K. H. Yoo, C. N. Whang, *Appl. Surf. Sci.* **2006**, *252*, 8015.

[38] J. Niederhausen, P. Amsalem, A. Wilke, R. Schlesinger, S. Winkler, A. Vollmer, J. P. Rabe, N. Koch, *Phys. Rev. B* **2012**, *86*, 081411.

[39] K. Akaike, K. Kanai, H. Yoshida, J. Tsutsumi, T. Nishi, N. Sato, Y. Ouchi, K. Seki, *J. Appl. Phys.* **2008**, *104*, 023710.

[40] Z. L. Guan, J. B. Kim, H. Wang, C. Jaye, D. A. Fischer, Y. L. Loo, A. Kahn, *Org. Electron* **2010**, *11*, 1779.

[41] B. P. Rand, J. G. Xue, S. Uchida, S. R. Forrest, *J. Appl. Phys.* **2005**, *98*, 124902.

[42] G. A. H. Wetzelaer, M. Kuik, M. Lenes, P. W. M. Blom, *Appl. Phys. Lett.* **2011**, *99*, 153506.

[43] P. de Bruyn, A. H. P. van Rest, G. A. H. Wetzelaer, D. M. de Leeuw, P. W. M. Blom, *Phys. Rev. Lett.* **2013**, *111*, 186801.

[44] O. Rubel, S. D. Baranovskii, W. Stolz, F. Gebhard, *Phys. Rev. Lett.* **2008**, *100*, 196602.

[45] C. Schwarz, S. Tscheuschner, J. Frisch, S. Winkler, N. Koch, H. Bässler, A. Köhler, *Phys. Rev. B* **2013**, *87*, 155205.

[46] K. J. Laidler, *Pure Appl. Chem.* **1996**, *68*, 149.

[47] J. Wagner, M. Gruber, A. Wilke, Y. Tanaka, K. Topczak, A. Steindamm, U. Hormann, A. Opitz, Y. Nakayama, H. Ishii, J. Pflaum, N. Koch, W. Brütting, *J. Appl. Phys.* **2012**, *111*, 054509.

[48] J. Nelson, J. Kirkpatrick, P. Ravirajan, *Phys. Rev. B* **2004**, *69*, 035337.

[49] S. Tscheuschner, H. Bässler, K. Huber, A. Köhler, *J. Phys. Chem. B* **2015**, *119*, 10359.

[50] S. Gelinas, A. Rao, A. Kumar, S. L. Smith, A. W. Chin, J. Clark, T. S. van der Poll, G. C. Bazan, R. H. Friend, *Science* **2014**, *343*, 512.

[51] A. A. Bakulin, A. Rao, V. G. Pavelyev, P. H. M. van Loosdrecht, M. S. Pshenichnikov, D. Niedzialek, J. Cornil, D. Beljonne, R. H. Friend, *Science* **2012**, *335*, 1340.

[52] S. Athanasopoulos, S. T. Hoffmann, H. Bässler, A. Köhler, D. Beljonne, *J. Phys. Chem. Lett.* **2013**, *4*, 1694.

[53] B. B. Y. Hsu, C. M. Cheng, C. Luo, S. N. Patel, C. Zhong, H. T. Sun, J. Sherman, B. H. Lee, L. Ying, M. Wang, G. C. Bazan, M. Chabinyc, J. L. Brédas, A. Heeger, *Adv. Mater.* **2015**, *27*, 7759.

[54] C. Schwarz, H. Bässler, I. Bauer, J. M. Koenen, E. Preis, U. Scherf, A. Köhler, *Adv. Mater.* **2012**, *24*, 922.

[55] G. Juska, N. Nekrasas, K. Genevicius, *J. Non-Cryst. Solids* **2012**, *358*, 748.

[56] A. Armin, G. Juska, M. Ullah, M. Velusamy, P. L. Burn, P. Meredith, A. Pivrikas, *Adv. Energy Mater.* **2014**, *4*, 1300954.